Final Report DOE-BES AMO Grant DE-FG02-04ER15592

Generation of Bright Soft X-ray Laser Beams
DOE-AMOS Grant DE-FG02-04ER15592

Jorge J. Rocca
Department of Electrical and Computer Engineering and Department of Physics
Colorado State University, Fort Collins, CO 80523-1373.
jorge.rocca@colostate.edu

Abstract

The project goal was to demonstrate new compact soft x-ray lasers emitting high energy ultrashort pulses at shorter wavelengths and increased repetition rates by amplification in atomic transitions in high density laser-created plasmas. To demonstrate these lasers we developed new high power solid state lasers (*IEEE J. Selected Topics in Quantum Electronics*, ***25***, *8800515, (2019)*). The project succeeded in demonstrating the shortest wavelength compact soft x-ray laser to date, 6.85 nm wavelength, and the highest repetition rate table-top soft x-ray laser, 400 Hz. We also applied these compact soft x-ray laser sources to determine the composition of materials with nanoscale resolution using a new technique that combines soft x-ray laser ablation with mass spectrometry, and we demonstrated that these lasers are capable of acquiring nanoscale resolution holograms with picosecond time resolution.

The combination of an increased pumping efficiency with increased repetition rates can yield soft x-ray laser beams with an unprecedented average power on a table-top for applications demanding a high photon flux. We have demonstrated that the efficiency of plasma-based laser-pumped soft x-ray lasers can be significantly increased by detailed pulse shaping of the pump laser using a new pulse synthesizer. Results include the demonstration of 18.9 nm wavelength laser operation at a record 400 Hz repetition rate, and the extension of repetitive gain-saturated plasma-based table-top x-ray lasers to the shortest wavelength to date, 6.85 nm *(Optica, **5**, 257, (2018))*. Laser amplification was also observed at wavelengths as short at 5.8 nm by isolectronic scaling in Ni-like lanthanide ions. We have also conducted simulations to explore the possibility of demonstrating gain saturated atomic x-ray lasers near the carbon K-edge, in the "carbon window" for the first time.

The work conducted under this program also includes the use of compact soft x-ray lasers in applications to problems of chemical interest, such as isotopic composition mapping of micron-size uranium particles with nanoscale resolution *(J. Analytical Atomic Spectrometry, **32,** 1092 (2017))*, and nanoscale resolution depth profiling analysis of CoNCN-coated electrodes for water oxidation catalysis. We also demonstrated single-shot high resolution soft x-ray Fourier transform holography over a broad 7 μm diameter field of view with ~ 5 ps temporal resolution *(Optics Express, **28**, 35898, (2020))*.

A summary of the results obtained under this grant is given below.

1. Demonstration of increased efficiency of table-top soft x-ray lasers sources by pump laser pulse shaping. We have succeeded in demonstrating a significant increase in the efficiency of table-top soft x-ray lasers by precise tailoring of the pump pulse. Previous research has shown that control of the rate at which the pump pulse energy is deposited to create and heat the plasma can greatly influence the magnitude of the gain, as well as its duration and spatial spread. However, precise control of the shape and duration of the entire pump pulse sequence has never been attempted despite its significant potential to improve the performance of soft x-ray lasers. This has been the case due to the difficulty of creating Joule-level pulses of arbitrary shape and simultaneously having picosecond features and total pulse duration spanning several nanoseconds.

To overcome this limitation, we have developed a pulse shaping technique with programmability for the generation of Joule-level pulses and pulse trains of arbitrary shapes up to 9 ns in duration. The pulse synthesizer is based in pulse stacking, a technique based on pulse splitting and recombination that has been used before, but that to the best of our knowledge, had not been shown to be capable of generating synthesized pulses of Joule-level energy with a record length greater than a few hundred picoseconds and with a resolution of a few picoseconds. Our new pulse synthesizer generated 1 J pulses of up to 9 ns in duration with a temporal resolution of 8 ps. The pulse synthesizer, illustrated in Figure 1, was inserted into a cryogenically cooled high power diode-pumped Yb:YAG laser system. It can generate trains of ten sub-pulses with peak powers of > 10 GW when all the sub-pulses are of equal amplitude. The pulse synthesizer consists of three functional modules: a two-stage cylindrical telescope, an array of liquid crystals, and a set of sliding retro-reflectors inserted into a high power cryogenically cooled diode-pumped Yb:YAG laser system composed of two room temperature regenerative amplifiers and a sequence of two cryogenically cooled Yb:YAG high power amplifiers. The pulse synthesizer was placed at the output of a first regenerative amplifier. The pulse entering the pulse synthesizer is linearly polarized, and the direction of polarization can be tuned using a λ/2 wave plate. The polarization state of each sub-pulse changes after it passes through a liquid crystal twice and-can be controlled by selecting the voltage applied to liquid crystal.

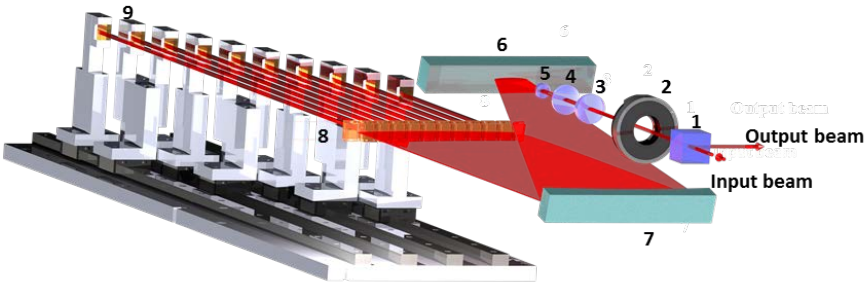

Figure 1 3-D schematic diagram of the pulse synthesizer for the generation of high energy laser pulses of arbitrary shape 1. Polarizing cube, 2. half-wave plate, 3. negative cylindrical lens, 4. positive cylindrical lens, 5. positive cylindrical lens, 6. flat mirror, 7. concave cylindrical mirror, 8. liquid crystals, 9. mobilized retroreflectors.

The synthesized pulses are injected into a second regenerative amplifier which increases their pulse energy to compensate for losses in the pulse shaper, improves their beam quality, and makes the sub-pulses co-linear as required for efficient further amplification and use. The synthesized pulse train is first amplified to ~100 mJ by the first of two cryogenically-cooled Yb:YAG amplifiers and is subsequently further amplified to 1.3 J by the second amplifier. These two stages of high power cryogenically-cooled Yb:YAG amplifiers are similar to those we demonstrated before as part of this project (C. Baumgarten et at, Optics Lett. **41**, 3339, (2016)). They are based on liquid nitrogen-cooled active mirror slabs operating in a multi-pass configuration.

Another advantage of this pulse shaping technique is that the synthesized high energy pulses are chirped and can be compressed into sub-pulses of picosecond duration by a grating pulse compressor. The cryogenically cooled Yb: YAG amplifiers have a bandwidth of ~ 0.3 nm, sufficient to allow compression into pulses of sub-5 ps duration.

Using this new pulse synthesizer we demonstrated tailoring the high energy pump pulses with an unprecedented degree of freedom. We are finding, as we expected, that the soft x-ray laser output energy is very sensitive to the shape of the pump pulses and that it can be optimized to achieve maximum conversion efficiency. This is illustrated for an 18.9 nm wavelength Ni-like Mo laser in Figure 2, in which a pump pulse sequence consisting of an early train of 8 picosecond duration pre-pulses precedes a low intensity nanosecond plateau followed by a sequence of two closely separated 8 picosecond pulses. The output energy 18.9 nm soft x-ray laser is measured to depend greatly on the characteristic of the early picosecond pulse train. In all cases the early picosecond pulse train contains 5 % or the total pump energy. However, when this pulse trains increases in complexity from a single pulse to three pulses separated by

50 ps, the soft x-ray laser output pulse energy increases from 0.03 μJ to 3.7μJ. The latter represents a factor of two increase in efficiency and pulse energy over the highest values we had previously achieved. The pump pulse optimization is still ongoing, exploiting the flexibility provided by the control of the amplitude and delay between ten picosecond duration pulses. Comparison with simulations will provide additional insight on the plasma physics and guide further optimization. Nevertheless, the result presented above already represents a record output for this type table-top lasers, and a promising approach to improve the efficiency of compact plasma-based x-ray lasers in general.

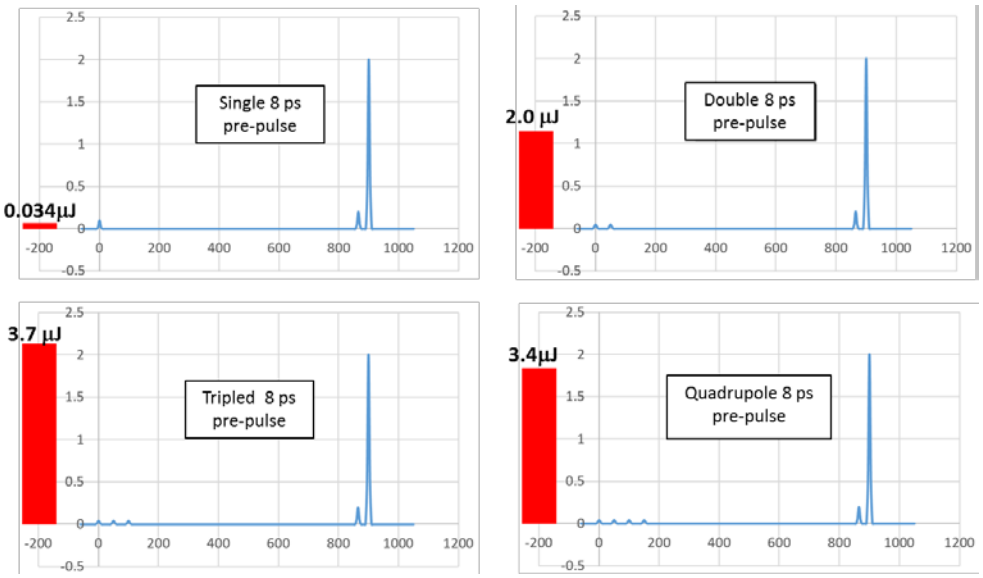

Figure 2. Output pulse energy of an 18.9 nm Ni-like Mo laser excited with different synthetized pulses (red bars). The pump pulses (blue traces) differ on the composition of the early train of 8 ps pre-pulses, that in all cases contains 5% of the total pump energy.

2. Simulations of atomic x-ray laser amplification in the carbon window. We have conducted simulations to explore the possibility of demonstrating gain saturated atomic x-ray lasers near the carbon K-edge, in the "carbon window" for the first time. Model simulations show that a direct extrapolation of the approach we successfully used to obtain strong lasing in the atomic transitions of Ni-like Gd (λ = 6.8nm) and other lanthanide elements during the present grant period would not provide sufficient gain. A reason for this is that as the degree of ionization of the plasma increases, as required to obtain lasing at shorter wavelengths in Ni-like ions, the electron density required to achieve the necessary electron impact excitation rate also increases. Lasing in atomic transitions with wavelengths in the "carbon window" requires an electron density that starts to approach the critical density, $n_{ec}=1.7x10^{21}$ cm^{-3} for the λ = 800 nm light from the Ti:Sa pump laser used. Consequently, in plasmas generated with near infrared pump lasers the region where x-ray amplification occurs is too close to the critical density

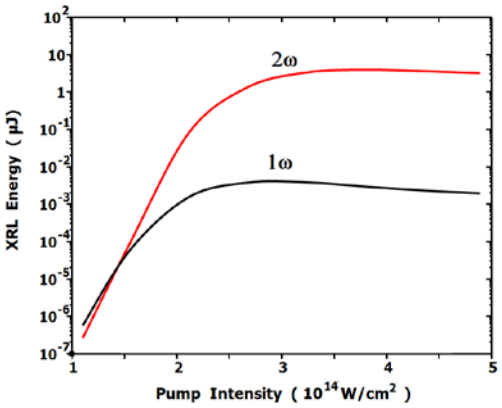

Figure 3. Comparison of the simulated output pulse energies for λ =4.5 nm Ni-like Ta 4d-4p x-ray laser as a function of pump intensity for: λ = 800 nm pump pulse (black curve) and a second harmonic pump pulse (red curve). Second harmonic pumping is key for the successful operation of the laser.

surface. In this region the electron density gradient is too step to allow for the amplified x-rays to travel the necessary distance through the gain medium without being refracted away. This results in very low amplification, leading to a very low output energy pulse (black line in Figure 3) for soft x-ray lasers on Ni-like ions of Ta operating near 4.5 nm.

To overcome this limitation, we explored departing from the traditional approach used in all the atomic plasma-based x-ray lasers demonstrated to date, and consisting of using the fundamental wavelength of the pump laser. Instead, we will use the second harmonic, $\lambda = 400$ nm, from a Ti:Sa pump laser. The shorter pump wavelength will increase by 4× the critical density to 6.9×10^{21} cm^{-3}. As a result, the optimum plasma region for x-ray amplification will occur in a plasma region with the required higher density but further from critical density region and hence reduced density gradient. Hydrodynamic atomic physics simulations we have conducted for a Ni-like lutetium Lu (Z=71) soft x-ray laser (λ=4.7 nm) in a line focus plasma generated with $\lambda = 400$ nm pump pulses of 40 ps duration impinging at near normal incidence onto solid targets at an intensity of 3×10^{14} W cm^{-2} predict a gain coefficient of ~ 50 cm^{-1}. This gain is sufficient to saturate the gain medium and generate pulse energies of several μJ. Similar gains are computed for other transitions at wavelengths between 4.26 nm and 5.8 nm from Ni-like ions ranging in Z from Er (Z=70) to W (Z=74). They cover the carbon window, and in the case of W the shortest wavelength transition is in the water window (λ~4.23 nm).

3. Demonstration of compact gain-saturated X-ray lasers down to 6.85 nm and gain down to 5.85 nm. During this grant we have succeeded in extending gain saturated repetitive x-ray lasers down to 6.85 nm in Ni-like Gd. These lanthanides ion-based collisionally pumped lasers generate micro joule pulses which enable, for example, nano-scale resolution single shot imaging, opening the opportunity to conduct sequential imaging of ultrafast nano-scale phenomena with ultra-high special resolution. In the same experiments, we also observed gain at even shorter wavelength transitions, down to 5.85 nm in Ni-like Dy. These results, in combination with previous measurements of the optimum angles for lasing in lower Z ions, allowed us to experimentally determine the optimum pump angle for laser operation at wavelengths between 18.9 nm and 5.85 nm, which is closely related to the plasma density at which lasing occurs. The results were useful to benchmark models that can be used to predict the optimum irradiation conditions necessary to further extend table-top gain saturated laser to even shorter wavelengths.

The soft x-ray lasers were excited by irradiating 1–2 mm thick solid slab targets with a sequence of two laser pulses from a λ=800 nm chirped pulse amplification Ti:Sa laser. The two-pulse sequence consisted of a normal-incidence pre-pulse followed by a main sub-picosecond pulse impinging at selected grazing incidence angles with a traveling-wave excitation velocity of $(1.0 \pm 0.03)c$. An acousto-optic programmable dispersive filter was used after the laser oscillator to tailor the bandwidth of the Ti:Sa pump laser. This gave us the ability to adjust the length of the un-compressed pre-pulse from 45 ps to 300 ps to find the optimal conditions for laser amplification, which was proven critical to obtain the results discussed below. The plasmas were created by normal-incidence irradiation at an intensity of $I \sim 2\times10^{13}$ W/cm^2 with a 185 ps duration pre-pulse. The pre-pulse was focused onto the target to form a line of approximately 15 μm FWHM width and ~ 9 mm length using the combination of a spherical and a cylindrical lens. To assist in achieving efficient pumping, we developed a focusing geometry designed to create a plasma column of constant width along the target. The plasma created by the pre-pulse is allowed to expand to reduce the density gradient and subsequently is rapidly heated with a ~ 7.2 J pulse of 0.7 ps FWHM duration. This pre-pulse is shaped into a line focus of approximately 30 μm × 9 mm FWHM, corresponding to an intensity of $I \sim 3.6\times10^{15}$ W/cm^2. The target surface was tilted with respect to the axis of the short pulse to define a grazing incidence angle of 35 degrees and 43 degrees for efficient heating in the case of Sm and Gd respectively. Due to the short duration of the gain, the mismatch between the propagation velocities of the pump pulse and the amplified soft x-ray laser pulse significantly reduces the amplification of the soft x-ray laser pulse. To overcome this limitation, a reflection echelon composed of six adjustable mirror segments was used to obtain traveling wave excitation.

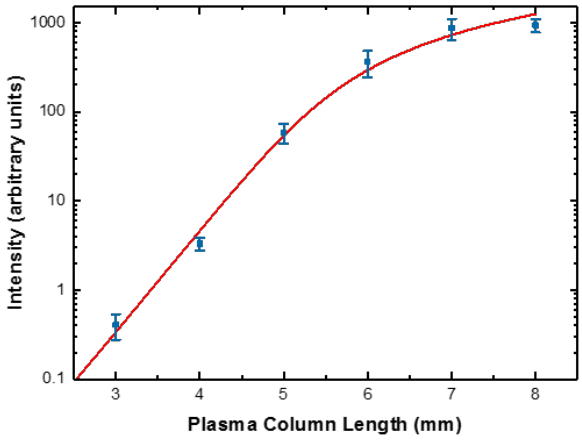

Figure 4. Intensity of the λ= 7.36 nm laser line of Ni-like Sm as a function of the plasma-column length. The red line is a fit of the data that yields a gain coefficient of 27.3 cm^{-1} and a gain-length product of 16.6. The error bar represents 1 standard deviation.

Figure 4 shows a 3 orders of magnitude increase in the intensity of the λ=7.36 nm 4d $^1S_0$-4p $^1P_1$ laser transition of Ni-like Sm as the plasma column length increases from 3 mm to 8 mm. Saturation of the gain is observed to have an onset at a plasma-column length of approximately 5.5 mm. A fit of the data with an expression for the gain that takes into account saturation yields a gain coefficient of 27.3 cm^{-1} with a gain-length product of 16.6. The energy of the most intense Sm laser pulses was estimated to be ~ 1.8 μJ from the CCD counts, a value that is sufficient to perform nano-scale imaging with a single laser shot. Similar pump pulse conditions were used to obtain a gain-saturated λ=6.9 nm laser in Ni-like Gd. Figure 5(a) shows a series of on-axis spectra as a function of the length for a Gd plasma column created by depositing 7.3 J of short- pulse energy and a total of 14.1 J optical pump pulse energy on a polished Gd slab target with the irradiation parameters described above. Figure 5.2(b) shows the increase in the 6.85 nm laser line intensity as a function of plasma column length. A fit to the data gives a gain coefficient of 26.3 cm^{-1} and a gain length product of 16.2. The pulse energy for the longest plasma column length is ~ 1 μJ. Weak amplification was also observed for λ= 6.85 nm and λ= 6.4nm of Ni-like Sm and Gd respectively. The results are in good agreement with hydrodynamic/atomic physics simulations.

The demonstration of a gain-saturated tabletop laser at λ= 6.85 nm with reduced pump energy also opens the prospect for bright high-repetition-rate plasma-based lasers at shorter wavelengths. In progress toward this goal, we made use of isoelectronic scaling along the elements of the lanthanide series to obtain lasing in several shorter wavelength transitions from Ni-like ions. The spectra of Figure 6 show that the use

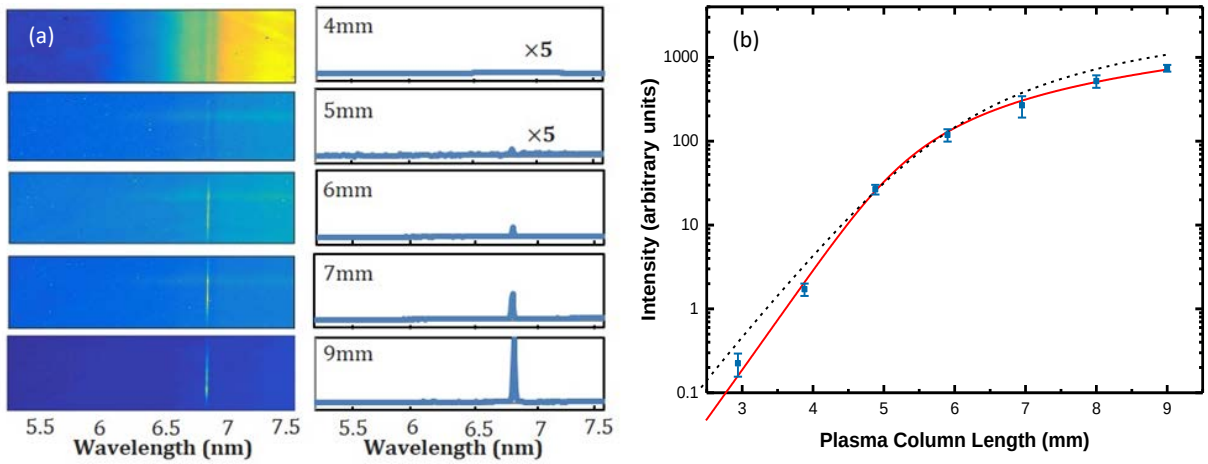

Figure 5. (a) End-on spectra of a line-focus Gd plasma column showing saturated amplification in the λ= 6.85 nm line of Ni-like Gd. With the first two integrations plots on the right multiplied by 5. **(b)** Intensity of the λ= 6.85 nm laser line as a function of the plasma-column length. The solid red line is a fit of the data that yields a gain coefficient of 26.3 cm^{-1} and a gain-length product of 16.2. The error bar represents 1 standard deviation. The black dashed line is the result of atomic physics/hydrodynamic simulation with a gain-length product of 16.9.

of similar irradiation conditions resulted in strong amplification in the λ= 6.6 nm and λ=6.0 nm transitions of Ni-like Tb. Finally, we have also observed amplification in the λ=5.85 nm and λ=6.4 nm lines of Ni-like Dy (Figure 6) using the same pump conditions. For lasing in all elements the traveling wave excitation was kept constant and near c. The spectra in Figure 6 show that the intensity ratio of the longer wavelength to the shorter wavelength of the two J=0-1 lines becomes smaller as Z increases, with the shortest wavelength line becoming dominant for Ni-like Dy.

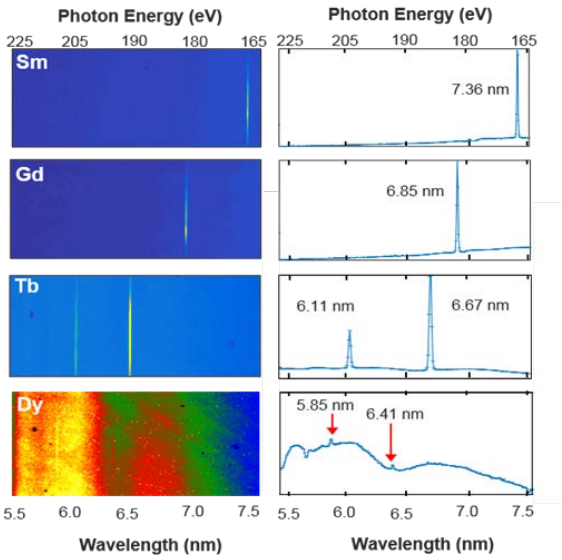

Figure 6. End-on spectra showing lasing at progressively shorter wavelengths in the $4d^1\ S_0$-$4p^1\ P_1$ line of nickel-like lanthanide ions, down to λ= 5.85 nm in nickel-like Dysprosium.

Another significant aspect of these amplifiers is the fact that collisional x-ray laser amplification at shorter wavelengths favors higher plasma densities. This is shown by the increase of the grazing incidence angle of the short pump pulse necessary for optimum laser amplification. Adding the experimental data of optimum angle obtained in this work to our previously published data for lower Z Ni-like ions, we were able to experimentally map the dependence of the optimum pump angle and plasma density for a large range of Z and lasing wavelengths, in comparison with simulations. This provides both a benchmark for simulation codes, as well as a prediction of the optimum condition for further scaling these lasers to shorter wavelengths. The increase in irradiation angle was observed to be linear over a broad range of atomic numbers ranging from Z= 42 (Mo) to Z=66 (Dy) (Figure 7). In this range of Z, the optimum short pulse irradiation angle is observed to increase from a grazing incidence angle of 17 degrees for Mo to 43 degrees for Dy. This corresponds to an increase in electron density from 1.5×10^{20} cm^{-3} to 7.9×10^{20} cm^{-3}.

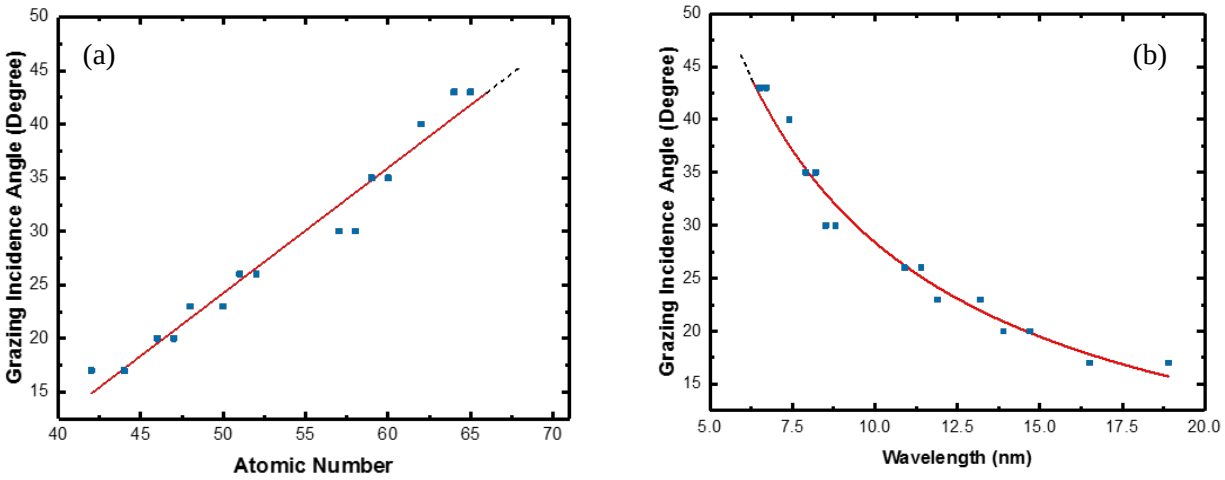

Figure 7. (a) Measured optimum grazing incidence angle as a function of atomic number. The dashed line is an extrapolation of the data. **(b)** The optimum grazing incidence angle as a function of lasing wavelength. The dashed line is an extrapolation of the data.

The results were modeled and analyzed with hydrodynamic/atomic physics simulations with the code Radex. A post processor ray tracing code was used to model the soft x-ray laser beam propagation along the plasma column. This allowed us to compute the gain saturation behavior, the role of refraction, the x-ray laser output pulse energy, and the beam divergence. To compute the small signal gain, the Ni-like ions were modeled with 287 levels including inner and outer shell levels. Other ions in vicinity of the Ni-like

were modeled using 300 single and doubly excited levels using atomic data and collisional rates from the code HULLAC. Ions far from the Ni-like state were modeled with just the lowest energy outer shell configuration plus the lowest inner shell and double excited levels. The atomic model was run self-consistently with the hydro code including up to 3000 levels. We observed that the computed gain decreases as the complexity of the atomic model and the number of levels is increased until the resulting gain becomes practically insensitive to a further increase in the number of levels. The dashed curve in Figure 8(a) is the result of the model simulations of the Gd 6.85 nm laser for the pump conditions used in the experiment assuming the width of the gain region in the direction parallel to the target is 10 μm. Good agreement with the experimental results is observed. The model predicts a beam divergence of 2.4 mrad in the directions parallel to the target, in good agreement with the measured value (see Figure 8(b)). The agreement with the experimental results allows us to use the simulations to further understand the operation of this x-ray laser amplifier. Figure 9 shows the computed spatial distribution of the beam intensity as a function of plasma column length. The model simulations show that in the case of the higher Z-ions refraction shifts the maximum gain to the lower density region where the electron density is (4 - 5) x 10^{20} cm^{-3}. At this density, the saturation intensity is computed to be 1.2×10^{10} W cm^{-2}. Simulations show this intensity is reached after the rays travel ~ 6 mm along the plasma column axis. The output intensity is computed to exceed the

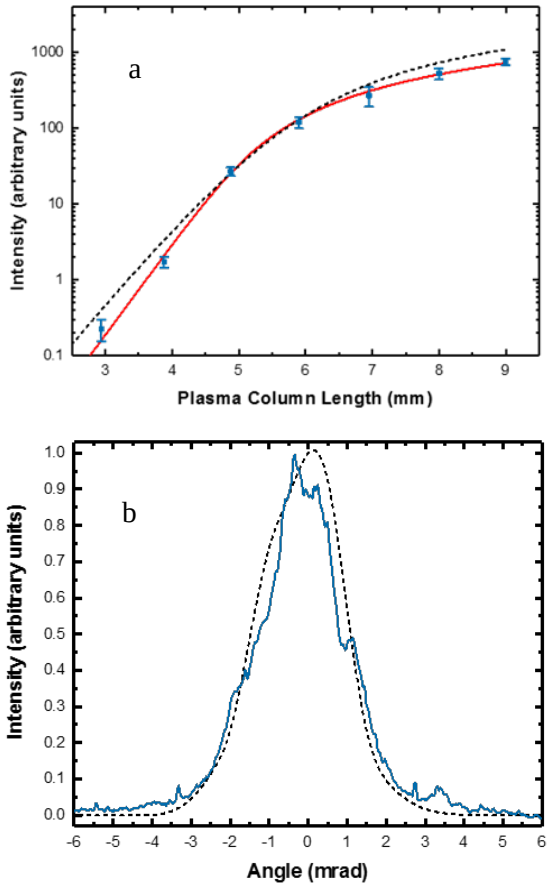

Figure 8 (a) Intensity of the λ= 6.85 nm laser line as a function of the plasma-column length. The solid red line is a fit of the data that yields a gain coefficient of 26.3 cm^{-1} and a gain-length product of 16.2. The black dashed line is the result of atomic physics/hydrodynamic simulation with a gain-length product of 16.9. **(b)** Measured (blue trace) and simulated (black dashed trace) Ni-like Gd laser far field beam intensity profile in the direction parallel to the target surface. The black dashed line is the modeled far field intensity, the FWHM beam divergence is ~ 2.4 mrad.

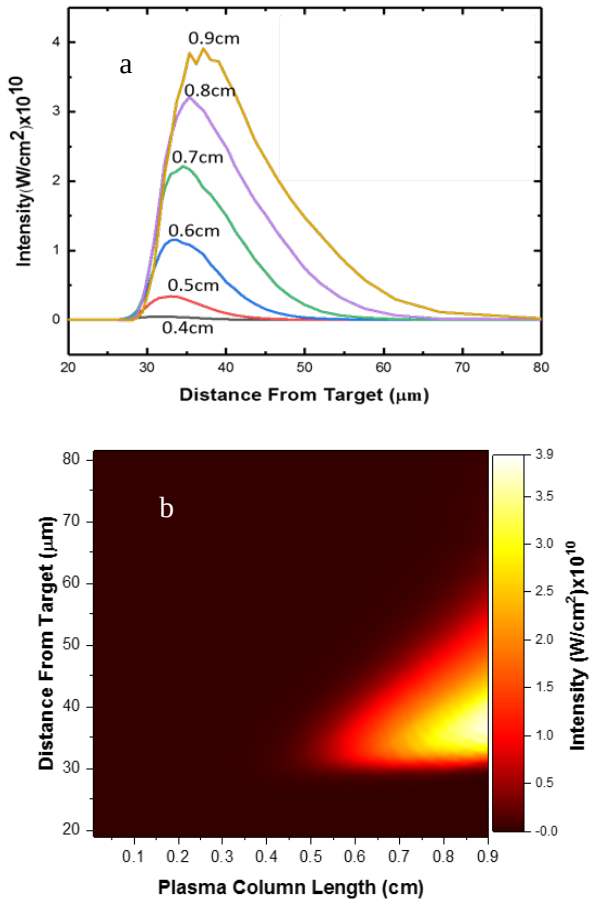

Figure 9. Computed evolution of the intensity distribution of the x-ray laser beam of the 6.85 nm line of Ni-like Gd as function of plasma column length. **(a)** Intensity vs distance to the target for increasing plasma column lengths between 0.4 and 0.9 cm. **(b)** Pseudo color map of the laser line intensity as a function of distance to the target and plasma column length.

saturation intensity by > 3× at the exit of the amplifier. Refraction is observed to shift the amplified beam progressively away from the target, decreasing the output pulse energy. The demonstration of a gain-saturated tabletop laser at λ= 6.85 nm in Ni-like Gd at this reduced pump energy also opens the prospect for bright high-repetition-rate plasma-based lasers at shorter wavelengths. In progress toward this goal, we used isoelectronic scaling along elements of the lanthanide series to obtain lasing in several other shorter wavelengths transitions from Ni-like ions at wavelengths as short as 5.85 nm in Ni-like Dy.

4. Nanoscale molecular composition imaging. During this grant we also have collaborated with scientists at Pacific Northwest National Laboratory (PNNL) in using one of our ultrashort wavelength lasers to map with nano-scale spatial resolution the isotopic composition of uranium micro-dust particles using a new ultrahigh resolution chemical composition imaging technique: Extreme Ultraviolet Time of Flight (EUV TOF) laser ablation mass spectrometry. Using as a benchmark the well-standardized NIST 61x glasses, the results show the EUV TOF spectra contain well defined signatures of U, Th, and their oxides, with far fewer spectral interferences than observed in Secondary Ion Mass Spectrometry Time of Flight (SIMS TOF). Furthermore, the method achieved a sample utilization efficiency (SUE), which is a measure of trace analysis sensitivity, of 0.014% for U and Th. This value compares very well with 0.017% of SIMS TOF in the same mass range. However, in imaging mode, EUV TOF is capable of mapping variations in composition with a superior lateral resolution of 80 nm. Such high lateral resolution enabled us to map the isotopic distribution of ^{238}U and ^{235}U in closely spaced micron-size uranium oxide particles from isotope standard materials (Figure 10). Trace elemental sensitivity and nanometer spatial resolution gives EUV TOF great potential to dramatically improve the state-of-the-art laser ablation/ionization mass spectrometry and elemental spectro-microscopy for applications such as geochemical, forensic and environmental analysis. The results are discussed in detail in a paper published in the Journal of Analytical Atomic Spectrometry[1].

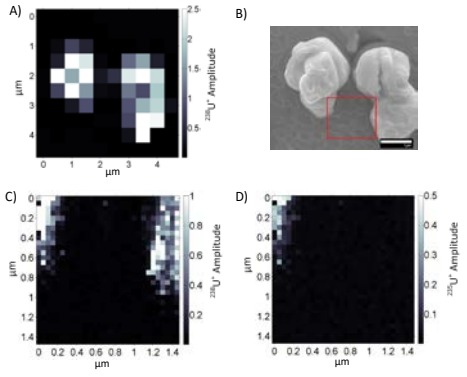

Figure 10. Isotopic Imaging of U micron size particles. **(A)** ^{238}U distribution. Pixel size: 200 nm. **(B)** Scanning electron micrograph of the particles. **(C)** ^{238}U distribution in the region delineated by the red square. Pixel size: 50 nm. **(D)** ^{235}U is only present in one of the particles. Pixel size: 50 nm.

5. Depth profile analysis of CoNCN for water oxidation catalyst by nano-ablation mass spectrometry with a compact extreme ultraviolet laser. We have used extreme ultraviolet (EUV) laser ablation time-of-flight mass spectrometry to conduct nano-scale depth resolution profiling analysis of a CoNCN-coated electrode for water oxidation catalysis *R. Muller et al., Anal Chem, **90**, 9234, (2018)*. The implementation of renewable hydrogen sources relies on the development of efficient catalysts for photo- and electro catalytic water splitting. The bottleneck of the overall efficiency is considered to be the thermodynamically demanding four-electron oxidation of water to molecular oxygen. Earth-abundant heterogeneous transition metal electro-catalysts improve the oxygen formation kinetics and are leading candidates for affordable large scale water electrolysis, both for the classical alkaline electrolyzers and direct photo-electro catalytic approaches. In order to allow targeted catalyst design and rational development, the catalytic mechanisms, reactive species, and structure-activity relationships remain to be elucidated. For electrochemical water oxidation catalysts based on transition metals, the formation of oxides or hydroxides on the electrode surface under turnover conditions is frequently debated and still a major concern. Even a monolayer of surface species can significantly alter the reaction processes that take place at the electrode-electrolyte interface. Among the relatively abundant transition metals, cobalt shows catalytic activity in various forms of oxides and hydroxides. We have used extreme ultraviolet (EUV) laser ablation time-of-flight mass spectrometry to conduct nano-scale depth resolution profiling analysis of a CoNCN-coated electrode for water oxidation catalysis. This method allowed us to distinguish different composite components of the

catalyst-Nafion blend, used to modify a screen-printed carbon electrode surface. Chemical information was extracted by fragment assignment and relative amplitude analysis of the mass spectrometry peaks. Pure Nafion and the exposed carbon substrate were compared as references. Material specific non-overlapping fragments were clearly identified by the detected mass-to-charge peaks of Nafion and CoNCN. 3D mapping of relevant mass peak amplitudes was used to determine the lateral distribution and to generate depth profiles from consecutive laser pulses (Figure 11). Evaluating the profiles of pristine electrodes gave insight into fragmentation behavior of the catalyst in a functional matrix.

Time of flight (TOF) mass spectra of EUV laser ablated pre- and post-catalytic CoNCN coated screen-printed electrodes for water oxidation revealed significant chemical depth profiling information. It was shown that the mass-to-charge peaks corresponding to N^+ as well as the ones correlated to the fragmentation of CoNCN ($CoCN^+$ and Co_2CN^+) and Nafion (CF^+, CF_3^+ and $C_3F_5^+$) are practically absent from the averaged mass spectra of the selected post-catalytic sample spots. Together with the increase in the C_2^+ amplitude, the results may indicate that these spots are devoid of a catalyst layer. On the other hand, Co^+ and N^+ are clearly detected on the first pulse, which shows that even small amounts of superficial catalyst remains above the substrate background. The confirmed localized absence of Nafion after electro catalysis provides valuable information to address possible layer-degradation and redeposition processes in a targeted way. Understanding the cause and process of electrode transformations is essential for the progress in catalyst development, especially for technological applications. To this end, also investigation of reference materials of different types and the impact of morphology and mixed materials requires additional attention. Overall, the sensitivity and spatial resolution we obtained fulfilled the required high demands of micro- to nanoscale electrode surface characterization, paving the way for a wider use of tabletop EUV lasers with TOFMS on chemistry applications beyond the field of electro catalysis

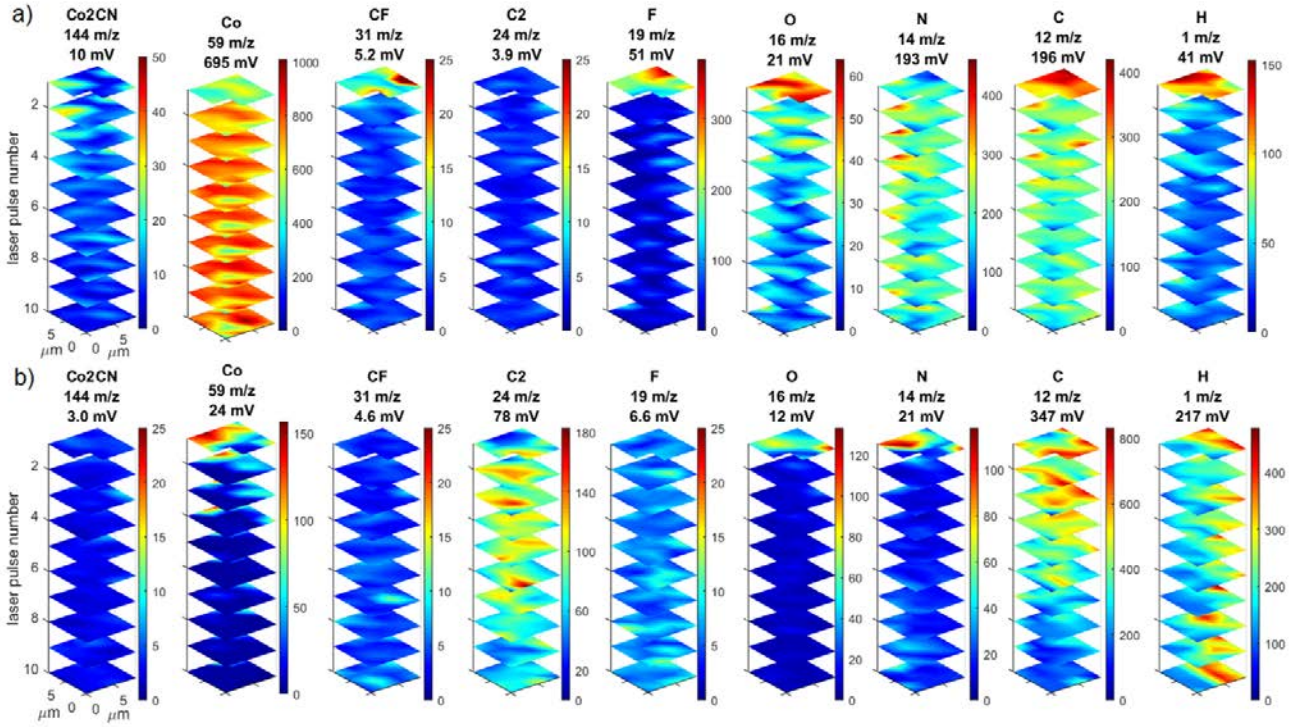

Figure 11. Depth profile representation of mass fragment peak areas by stacked 2D maps for a) pre-catalytic and b) post-catalytic CoNCN@Nafion coated SPEs. Below the peak assignment the rounded nominal mass and the average peak area is noted. The peak area magnitude is represented by color and is normalized to the corresponding signal maximum and set to 1 mV×ns for lower signals. Note the significant decrease of peak area and the adjusted scale for N^+, F^+ and Co^+ in the post catalytic sample.

6. Single-shot large field of view Fourier transform holography with a picosecond plasma-based soft X-ray laser A limitation of table-top soft x-ray sources in recording dynamic

nanoscale phenomena that are not necessarily periodic is to insufficient number of photons in a single shot. This can be solved the sue of a compact soft x-ray laser, of the type discussed in above in (1). We demonstrated single-shot high resolution Fourier transform holography over a broad 7 μm diameter field of view with ~ 5 ps temporal resolution. The experiment used a plasma-based soft X-ray laser operating at 18.9 nm wavelength with nearly full spatial coherence and close to diffraction-limited divergence implemented utilizing a dual-plasma amplifier scheme. The Fresnel holography set up is illustrated in Figure 12. A Fresnel zone plate with a central aperture is used to efficiently generate the object and reference beams. Rapid numerical reconstruction by a 2D Fourier transform allows for real-time imaging. Holograms with a half-pitch spatial resolution of 62 nm were obtained. Figure 13 compares single shot holographic images of silver nanowires obtained with this technique with scanning electron microscope images. While these are images of static object, this single-shot nanoscale-resolution imaging technique will allow for real-time ultrafast imaging of dynamic phenomena in compact setups. The field of view achieved covers an area of 38.5 μm^2 that is significantly larger than that of previous experiments. With the recent demonstration of sub 8 nm wavelength gain-saturated plasma-based table-top soft x-ray laser achieved as part this project, it will be possible to further improve the resolutions both in time and space using compact table-top systems. The single shot capability and rapid fast Fourier Transform reconstruction will allow the real time recording of ultrafast dynamic phenomena at the table-top scale. The results were published in *Optics Express, **28**,35898 (2020).*

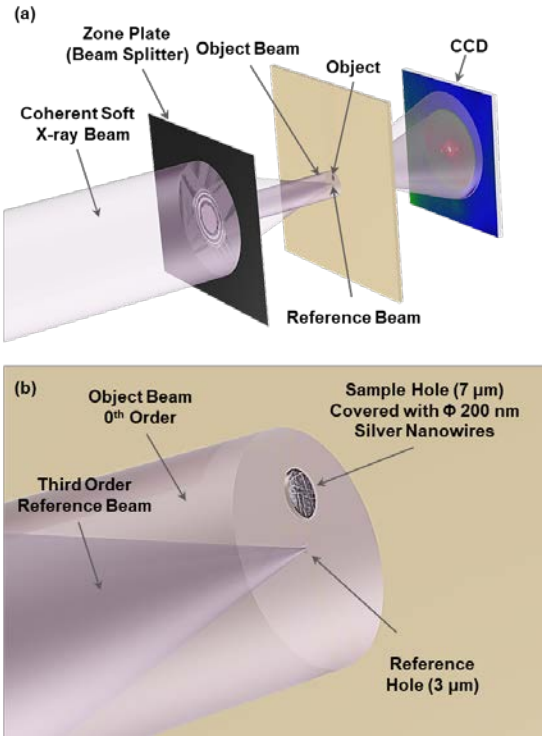

Figure 12. (a) Schematic representation of the Fourier holography setup. A zone plate is used as a beam splitter. The mask contains a hole to define the reference beam and a semitransparent area to support the sample. The recording is performed with a CCD. (b) Zoom of the sample plane showing beam that illuminates the sample and the refence beam.

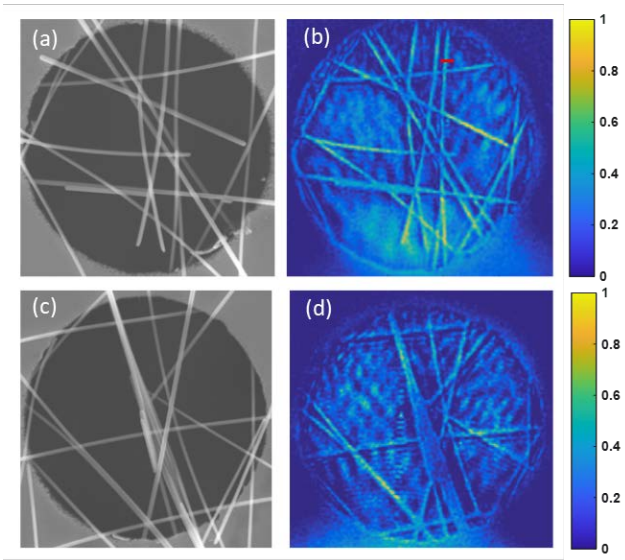

Figure 13. Electron microscope image (a), (c) and corresponding single shot holographic images (b), (d) of the silver nanowires over a 7 μm diameter hole.

7. Amplification of elliptically polarized sub-femtosecond pulses in a neon-like active medium of a plasma based X-ray laser modulated by an IR field. We also collaborated with the group of Prof. Olga Kocharovskaya (Texas A&M) in investigating of an scheme for the generation of high energy attosecond pulses of XUV radiation with elliptical or circular polarization, as well as the possibility of controlling the ellipticity of the amplified XUV pulses. The method consists in amplifying a train of sub-femtosecond pulses of extreme ultraviolet (XUV) radiation with a circular or elliptical polarization, constituted by high-order harmonics of an infrared (IR) laser field, in a neon-like active medium of a plasma-based X-ray laser that is additionally irradiated with a replica of a fundamental frequency laser field used to generate harmonics. The possibility of controlling the ellipticity of high-harmonic radiation (including increasing the ellipticity) during the amplification process was theoretically shown both for a single harmonic and a sub-femtosecond pulse train. The experimental implementation is suggested in an active medium of a plasma soft x-ray laser based on neon-like Ti^{12+} ions irradiated by an IR laser field with a wavelength of 3.9 μm.

Journal Publications Resulting from DOE-AMOS Grant DE-FG02-04ER15592

1. Shoujun Wang, Alex Rockwood, Yong Wang, Wei-Lun Chao, Patrick Naulleau, Huanyu Song, Carmen S. Menoni, Mario Marconi, and Jorge J. Rocca , "Single-shot large field of view Fourier transform holography with a picosecond plasma-based soft X-ray laser ", Optics Express, 35898**, 28**, (2020)
2. S. Wang, C.M. Baumgarten, Y. Wang, B.A. Reagan, A.P. Rockwood, H. Wang, L. Yin, K. Wernsing, H. Bravo, B.M. Luther, C.S. Menoni and J.J. Rocca, "High-Power Ultrashort Pulse Lasers to Pump Plasma-Based Soft X-Ray Lasers," IEEE J. Selected Topics in Quantum Electronics, **25**, 8800515, (2019) *(Invited Paper)*.
3. Rockwood, Y. Wang, S. Wang, M. Berrill, V.N. Shlyaptsev, and J.J. Rocca, "Compact gain-saturated x-ray lasers down to 6.85 nm and amplification down to 5.85 nm". Optica. **5**, 257, (2018).
4. R. Muller et al., "Depth-Profiling Microanalysis of CoNCN Water-Oxidation Catalyst Using a l=46.9 nm Plasma Laser for Nano-Ionization Mass Spectrometry," Analytical Chemistry, **90**, 9234, (2018).
5. A.Rockwood, Y. Wang, S. Wang, V.N. Shlyaptsev, J. J. Rocca, and M. Berrill, "Compact Gain-Saturated X-ray Lasers Down to 6.85 nm". Optics & Photonics News. **29**, (2018).

6. V. Vozda, et al. "Micro-Raman mapping of surface changes induced by XUV laser radiation in cadmium telluride," J. Alloys and Compounds, **763**, 662 (2018).
7. L. Vysin, T. Burian, E. Ukraintsev, M. Davidkova, M.E. Grisham, S. Heinbuch, J. J. Rocca, and L. Juha, "Dose-Rate Effects in Breaking DNA Strands by Short Pulses of Extreme Ultraviolet Radiation," Radiation Research, Vol. **189**, 466-476, (2018)
8. T. Green et al, "Characterization of extreme ultraviolet laser ablation mass spectrometry for actinide trace analysis and nanoscale isotopic imaging", J. of Analytical Atomic Spectrometry**, 32,** 1092-1100 (2017).
9. Baumgarten, M. Pedicone, H. Bravo, H.C. Wang, L. Yin, C.S. Menoni, J.J. Rocca, B.A. Reagan, "1 J, 0.5 kHz repetition rate picosecond laser", Optics Letters **41**, 3339 (2016).
10. V. Aslanyan, I. Kuznetsov, H. Bravo, M. R. Woolston, A. K. Rossall, C. S. Menoni, J. J. Rocca, and G. J. Tallents, "Ablation and transmission of thin solid targets irradiated by intense extreme ultraviolet laser radiation", Applied Physics Letters Photonics, **1,** 066101 (2016).
11. Y. Wang, S. Wang, E. Oliva, L. Lu, M. Berrill, L. Ying, J. Nejdl, B. Luther, C. Proux, T.T. Le, J. Dunn, D. Ros, P. Zeitoun, J. J. Rocca, "Gain dynamics in a soft X-ray laser amplifier perturbed by a strong injected X-ray field," Nature Photonics **8,** 381 (2014)

Other Publications Resulting from DOE-AMOS Grant DE-FG02-04ER15592

1. J.J. Rocca, B.A. Reagan, C. Baumgarten, Y. Wang, S. Wang, M. Pedicone, M. Berrill, V.N. Shlyaptsev, C.N. Kyaw, L. Yin, H. Wang, M.C. Marconi, C.S. Menoni, "Progress in high repetition rate soft x-ray laser development and pump lasers at Colorado State University," Proc. SPIE 10243, X-ray Lasers and Coherent X-ray Sources: Development and Applications, 102430F (2017). (Invited)
2. B. A. Reagan; C. M. Baumgarten; M. A. Pedicone; H. Bravo; L. Yin; M. Woolston; H. Wang; C. S. Menoni; J. J. Rocca, "Development of a kilowatt-class, Joule-level ultrafast laser for driving compact high average power coherent EUV/soft x-ray sources", Proc. SPIE 9740, Frontiers in Ultrafast Optics: Biomedical, Scientific, and Industrial Applications XVI, doi:10.1117/12.2212790 (2016)
3. C. M. Baumgarten, B. A. Reagan, M. Pedicone, H. Bravo, L. Yin, H. Wang, M. Woolston, B. Carr, C. Menoni, and J. Rocca, "Demonstration of a Compact 500 Hz Repetition Rate Joule-Level Chirped Pulse Amplification Laser," in *Conference on Lasers and Electro-Optics*, OSA Tech. Digest STu3M.3 (2016). (Invited)
4. B.A. Reagan, C. Baumgarten, K.A. Wernsing, M. Berrill, M. Woolston, L.Urbanski, W. Li, M.C. Marconi, C.S. Menoni, and J.J. Rocca, "Advances in High Average Power, 100 Hz Repetition Rate Table-top Soft X-ray Lasers), Springer Proc. in Physics, Vol. 169, X-Ray Lasers 2014, pp. 11-19 (2016). (Invited)
5. L. Li, et al., "Wave front study of fully coherent soft X-ray laser using Hartmann sensor", Springer Proceedings in Physics, Vol. 169, X-Ray Lasers 2014, pp 323-330 (2016).
6. B.A. Reagan, C. Baumgarten, M. Berrill, K.A. Wernsing, M. Woolston, L. Urbanski, W. Li, M.C. Marconi, V.N. Slyaptsev, C.S. Menoni, and J.J. Rocca, "Advances in High Average Power, 100 Hz Repetition Rate Table-Top Soft X-Ray Lasers" in Soft X-Ray Lasers 2014, Springer International Publishing (2016).

Invited Conference Presentations

1. J.J. Rocca, "Bright Coherent and Incoherent X-ray Generation at Colorado State University", 17th International Conference on X-Ray Lasers, Zurich (on line), December 2020.

2. J.J. Rocca, “Compact gain-saturated x-ray lasers down to 6.8 nm,” Winter Colloquium on the Physics of Quantum Electronics, Snowbird, Utah, January 6-11 (2019).

3. J.J. Rocca, et al., "Progress in high repetition rate soft x-ray laser development and pump lasers at Colorado State University," SPIE Conference on X-ray Lasers and Coherent X-ray Sources: Development and Applications, 1, San Diego, July 5 (2017).

4. J.J. Rocca, B. A. Reagan, C. Baumgarten, Y. Wang, S. Wang, A. Rockwood, M. Pedicone, L. Yin, H. Wang, M. Berrill, V.N. Shlyaptsev, C.S. Menoni, “High Average Power Table-Top Soft X-Ray Lasers and Their Enabling Pump Laser Technology”, 47th Winter Colloquium on the Physics of Quantum Electronics, January 8-13, Snowbird, Utah, (2017).

5. C.S. Menoni, M.C. Marconi, Y. Wang, S. Wang, A. Rockwood, C.N. Kyaw, I. Kuznetsov, T. Green, A. Duffin, J.J. Rocca, “The multiple facets of nanoscale imaging using soft x-ray light from bright table-top lasers”, 47th Winter Colloquium on the Physics of Quantum Electronics, January 8-13, Snowbird, Utah, (2017).

6. J. J. Rocca, "Table-top Soft X-Ray Lasers," in Conference on Lasers and Electro-Optics, OSA, San Jose, (2016).

7. B. A. Reagan et al., “Development of a kilowatt-class, joule-level ultrafast laser for driving compact high average power coherent EUV/soft x-ray sources. SPIE Conference on Frontiers in Ultrafast Optics: Biomedical, Scientific, and Industrial Applications XVI, 14-16 February, San Francisco, California (2016).

8. J.J. Rocca, “Soft X-Ray Lasers and their Applications”, tutorial delivered at the IEEE Photonics Conference (IPC), Orlando, Florida, October 1-5 (2017).

9. J.J. Rocca, B.A. Reagan, C. Baumgarten, Y. Wang, S. Wang, M. Pedicone, M. Berrill, Shlyaptsev, C.N. Kyaw, L. Yin, H. Wang, M.C. Marconi, C.S. Menoni, "Progress in high repetition rate soft x-ray laser development and pump lasers at Colorado State University," SPIE Conference X-ray Lasers and Coherent X-ray Sources: Development and Applications, July 5, San Jose, California (2017).

10. J.J. Rocca, “1 Joule, kilowatt-class average power, diode pumped ultrafast laser to drive soft x- ray lasers”, 7th Conference of the International Committee on Ultrahigh Intensity Lasers, September 11-16, Montebello, Quebec, Canada (2016).

11. J.J. Rocca, B.A. Reagan, C. Baumgarten, M. Pedicone, R. Hollinger, M.G. Capeluto, V.N. Shlyaptsev, V. Kaymak, A. Pukhov, C. Bargsten, Y. Wang, S. Wang, A. Rockwood, M. Berrill, C.S. Menoni, “Advances in compact soft X-ray lasers and bright X-ray generation from relativistic plasmas**”,** Proceedings VI International Conference, Frontiers of Nonlinear Physics, p41, July 17-23, Nizhny Novgorod, Russia (2016). Plenary talk

12. J.J. Rocca, B.A. Reagan, C. Baumgarten, M. Pedicone, R. Hollinger, M.G. Capeluto, C. Bargsten, V.N. Shlyaptsev, V. Kaymak, A. Pukhov, Y. Wang, S. Wang, A. Rockwood, M. Berrill, C.S. Menoni, “High Repetition Rate Soft X-Ray Lasers and Bright Table-top X-Ray Sources from Nanostructured Target Plasmas Irradiated at Relativistic Intensities”, OSA’s High-Brightness Sources and Light-Driven Interactions Congress, Long Beach, California, March 20-22, (2016).

13. J.J. Rocca, B.A. Reagan, C. Baumgarten, M. Pedicone, L. Yin, V.N. Shlyaptsev, Y. Wang, S. Wang, A. Rockwood, M. Berrill, M. Marconi, C.S. Menoni, “High Average Power Table-Top Soft X-Ray Lasers Using Diode-Pumped Laser Drivers”, 15th International Conference on X-Ray Lasers 2016, Nara-city, Japan, May 22-27, (2016).

14. B.A. Reagan, C.M. Baumgarten, M.A. Pedicone, H. Bravo, L. Yin, H. Wang, C.S. Menoni, and J.J. Rocca, "Development of High Repetition Rate, High Energy Diode-Pumped Short Pulse Lasers and Applications" in *Laser Congress 2017 (ASSL, LAC)*, Nagoya, Aichi: Optical Society of America (2017).

15. C. M. Baumgarten, et al., "Demonstration of a Compact 500 Hz Repetition Rate Joule-Level Chirped Pulse Amplification Laser," in Conference. on Lasers and Electro-Optics, OSA, (2016).

16. J.J. Rocca, B. Reagan, C. Baumgarten, Y. Wang, S. Wang. A. Rockwood, L. Yin, M. Marconi, V. Shlyaptsev, C. Menoni, “Towards milliwatt average power table-top soft x-ray lasers”, SPIE: X-Ray Lasers and Coherent X-Ray Sources: Development and Applications XI, 9-13 August, San Diego, California (2015).

17. J.J. Rocca, B.A. Reagan, C. Baumgarten, Y. Wang, S. Wang, A. Rockwood, L. Yin, M.C. Marconi, V.N. Shlyaptsev, and C.S. Menoni, "High Average Power Table-top Soft X-Ray Lasers" in *Advanced Lasers and Photon Sources*, Yokohama, Japan (2015).

Contributed Conference Presentation

A.P. Rockwood, Y. Wang, S. Wang, V.N. Shlyaptsev, M. Berrill, H. Song, and J. J. Rocca, "Compact Gain-Saturated Plasma-Based X-Ray Lasers Down to 6.85 nm and Amplification Down to 5.85 nm" in *International Conference on Plasma Science*, Denver, Colorado: IEEE P2A1346-93 (2018).

Ph.D students graduated

Cory Baumgarten: Ph.D in Physics, (2019)

Alex Rockwood: Ph.D in Physics. (2020)